Available online at www.sciencedirect.com
ScienceDirect
Journal of Nuclear Materials 372 (2008) 394–399
journal of nuclear materials
www.elsevier.com/locate/jnucmat

Sintering behavior of U–80 at.%Zr powder compacts in a vacuum environment

Tae-Kyu Kim *, Chong-Tak Lee, Dong-Seong Sohn

Advanced Nuclear Fuel Development Division, Korea Atomic Energy Research Institute, P.O. Box 105, Yuseong, Daejeon 305-600, Republic of Korea

Received 27 June 2006; accepted 8 April 2007

Abstract

Sintering behavior of U–80 at.%Zr powder compacts in a temperature range from 1100 to 1500 °C in a vacuum of 1×10^{-4} Pa was evaluated. The sintered density depended more on the sintering temperature than on the sintering time. The sintered specimens consisted of the δ-UZr_2 matrix with acicular α-Zr precipitates, but it still had un-reacted zirconium when the sintering temperature was 1100 °C. The uranium depletion near the surface of the specimens sintered at temperatures above 1300 °C was detected. Massive Zr(O) grains in the sintered specimen were found, and their formation was restrained when the cooling rate from the sintering temperature was increased.

PACS: 81.20.Ev; 65.40.De

1. Introduction

Metallic nuclear fuels can be utilized in the future light water reactors due to their excellent thermal conductivity. In particular, the metallic fuel with a composition of U–80 at.%Zr has drawn an attention as a nuclear fuel for advanced integral reactors [1]. In order to fabricate this fuel, a powder sintering method can be considered since the liquidus of U–80 at.%Zr is too high for the usual injection casting of the fast-reactor metal fuel. The sintering temperature is thus important as it can determine the physical properties of sintered fuels.

In this study, the sintering behavior of U–80 at.%Zr powder compacts in a temperature range from 1100 to 1500 °C in a vacuum was evaluated. The effect of the cooling rate from the sintering temperature on the microstructure was also evaluated.

2. Experimental procedure

Uranium powders were manufactured by a centrifugal atomizing process, and zirconium powders were prepared by a hydride–dehydride process. Impurity contents of the uranium and zirconium powders are given in Tables 1 and 2, respectively. Within a glove box filled with a purified argon gas, 20 at.% uranium and 80 at.% zirconium powders were mixed together in a V-type off-axis rotating mixer at 75 rpm for 2 h. The mixed powders were uniaxially cold compacted by using a double action press. In order to find the optimum compaction conditions, the compaction pressure was varied from 86 to 428 MPa with a fixed holding time of 20 s, and the holding time under the fixed pressure of 428 MPa was changed from 0 to 180 s. The sintering was then carried out at 1450 and 1500 °C for 2 h. The selected compaction conditions, a pressure of 428 MPa and a holding time of 20 s, were applied to other compaction experiments. The powder compacts were transferred to an alumina crucible in a vacuum chamber for the sintering (Fig. 1). The sintering was carried out at 1100, 1300, 1350, 1400, 1450 and 1500 °C with a cooling rate

* Corresponding author. Tel.: +82 42 868 8384; fax: +82 42 868 8346.
E-mail address: tkkim2@kaeri.re.kr (T.-K. Kim).

0022-3115/$ - see front matter © 2007 Elsevier B.V. All rights reserved.
doi:10.1016/j.jnucmat.2007.04.043

Table 1
Chemical composition of the impurities of the uranium powder (ppm)

Li	Al	Cu	Cd	O	C	N	H
<1.3	<600	<80	<10	<3000	<300	<500	<10

of 2 °C/min in a vacuum of about 1×10^{-4} Pa. An additional specimen sintered at 1500 °C was cooled down at a rate of 10 °C/min to observe the effect of the cooling rate on the microstructure of the sintered specimen.

After the sintering, the sintered density was measured, and the solid phases were identified by using a X-ray diffraction (XRD). The microstructure was examined by using both a scanning electron microscope (SEM) for a compositional contrast by using a back scattered electron image and an image analyzer (IA). Elemental analyses on the cross section of a sintered specimen were made by an energy dispersive spectroscope (EDS), and the homogeneity was investigated through the atomic ratio of U/Zr. The deposits on the inner surface of the crucible were also analyzed by using SEM/EDS. A Vickers hardness measurement of the sintered specimen was carried out.

3. Results and discussion

The SEM images of the uranium and zirconium powders are shown in Fig. 2. The uranium particles exhibited nearly a spherical shape with a smooth surface, representing the characteristics of centrifugally atomized powders (Fig. 2(a)). On the other hand, the zirconium particles revealed a porous surface, indicating the characteristics of hydride–dehydride processed powders (Fig. 2(b)). The mean particle sizes of the uranium and zirconium powders were 48 and 88 μm, respectively.

The effect of the compaction pressure on the green and sintered densities of the U–Zr specimen is shown in Fig. 3. It was found that the increase in the compacting pressure led to the increase in the green and sintered densities, and the highest sintered density was achieved at the maximum compacting pressure of 428 MPa.

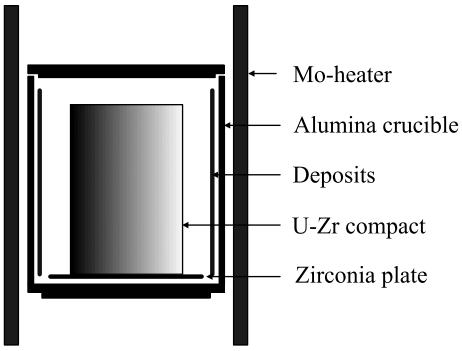

Fig. 1. Schematic drawing of the sintering of U–Zr powder compacts in a vacuum furnace.

The effect of the holding time under a compaction pressure of 428 MPa on the green and sintered densities of the U–Zr specimen is shown in Fig. 4. Compared with the results without a holding time under a compaction pressure, the green and sintered densities increased after the applied pressure was held for 20 s, and the densities remained constant as the holding time increased from 20 to 180 s. It is considered that a holding time of 20 s is long enough for the best densification.

The sintered density of the sintered specimen is given in Table 3. The sintered density increased continuously with an increasing temperature, and depended more on the sintering temperature than on the sintering time.

The X-ray diffraction patterns of the sintered U–Zr specimens are plotted in Fig. 5. As expected from the U–Zr phase diagram [2], the specimen consisted of two phases; δ-UZr_2 (hcp, $a = 0.5030$ nm, $c = 0.3080$ nm) and α-Zr (hcp, $a = 0.3232$ nm, $c = 0.5147$ nm).

Table 2
Chemical composition of the impurities of the zirconium powder (ppm)

Fe	Al	Cu	Mn	Ni	B	Si	Hf	Co	Cr	Ti	W	O	C	N	H
201	19	<10	<25	<30	0.5	<10	<100	<10	65	<25	43	<4000	34	<100	<50

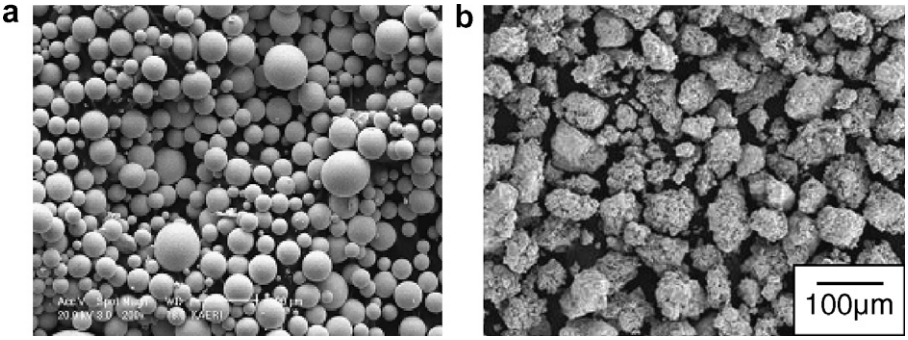

Fig. 2. SEM images of (a) uranium and (b) zirconium powders.

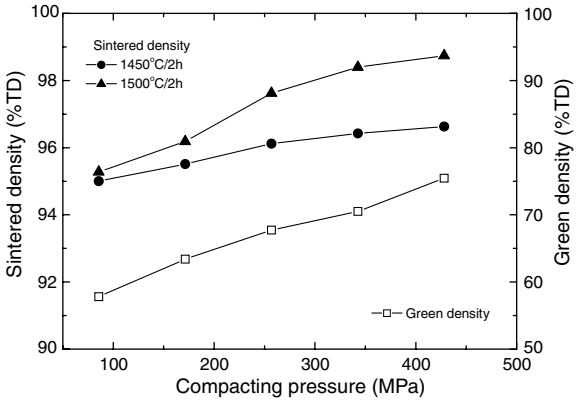

Fig. 3. Effect of the compaction pressure on the green and sintered densities of the U–Zr specimen.

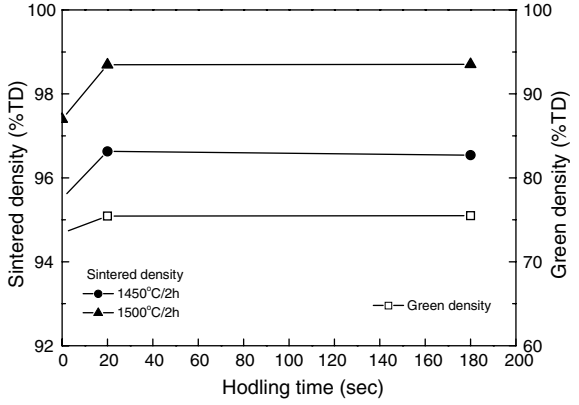

Fig. 4. Effect of the holding time under a compaction pressure of 428 MPa on the green and sintered densities of the U–Zr specimen.

The microstructures of the sintered specimens are shown in Fig. 6. The specimens consisted of the δ-UZr_2 matrix with acicular α-Zr precipitates. However, the specimen sintered at 1100 °C still had un-reacted zirconium particles (Fig. 6(a)), indicating that the sintering was not complete although the sintering at this temperature was carried out for as long as 100 h. Small amount of pores was also observed in the sintered specimens.

The area fraction of the pore and the mean pore area with a sintered density are plotted in Fig. 7. It was found that both the decrease in the area fraction of the pore and the pore coarsening accompanied the increase in the sintered density.

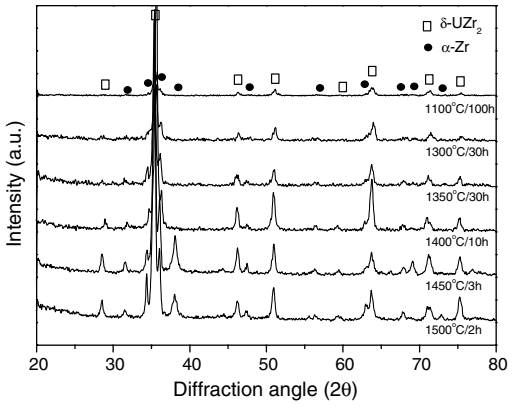

Fig. 5. X-ray diffraction patterns of the sintered specimens.

The atomic ratio of U/Zr in the cross section of the sintered specimen is plotted in Fig. 8. The atomic ratio of U/Zr in the specimen sintered at 1100 °C was almost constant, but it decreased by increasing the sintering temperature. Uranium depletion was detected up to about 1000 μm from the specimens' surface. It could be attributed to a vaporization of the U–Zr powder compacts during the sintering, thus forming deposits on the surface of the crucible (Fig. 1).

The SEM/EDS results of the deposits on the inner surface of the crucible after the sintering at 1500 °C for 2 h are shown in Fig. 9. The deposits were composed entirely of fine grains (Fig. 9(a)), and their chemical composition was found to be (in at.%) 17.52U, 5.99Zr and 76.49O (Fig. 9(b)). The vapor pressures of uranium and zirconium at 1500 °C have been reported to be about 2.8×10^{-2} and 3.5×10^{-5} Pa, respectively [3]. The mechanism leading to the deposits in the vacuum of 1×10^{-4} Pa is not clear yet. However, it is suspected that the vapor species other than U(g) and Zr(g) are involved, which may include ZrO(g) and UO(g) [4,5].

The effect of the cooling rate from a sintering temperature of 1500 °C on the microstructure of the sintered specimen is shown in Fig. 10. Massive grains were detected in the periphery of the specimen with a slow cooling rate of 2 °C/min (Fig. 10(a)). Its chemical composition was found to be (in at.%) 86.62Zr, 13.38O (Fig. 10(c)). The grains of

Table 3
Sintered density of the sintered specimen

Temperature (°C)	Time (h)	Powder compact			Sintered alloy				
		Diameter (mm)	Length (mm)	Weight (g)	Diameter (mm)	Length (mm)	Weight (g)	Density (g/cm^3)	%TD
1100	100	25.0	35.03	107.81	24.27	33.55	107.77	8.04	92.7
1300	30	25.0	34.91	107.80	24.08	33.25	107.68	8.18	94.3
1350	30	25.0	34.88	107.79	23.59	32.78	107.63	8.44	97.3
1400	10	25.0	34.85	107.79	23.59	32.74	107.62	8.47	97.7
1450	3	25.0	35.08	107.81	23.57	32.96	107.59	8.50	98.0
1500	2	25.0	34.97	107.76	23.56	32.82	107.52	8.56	98.7

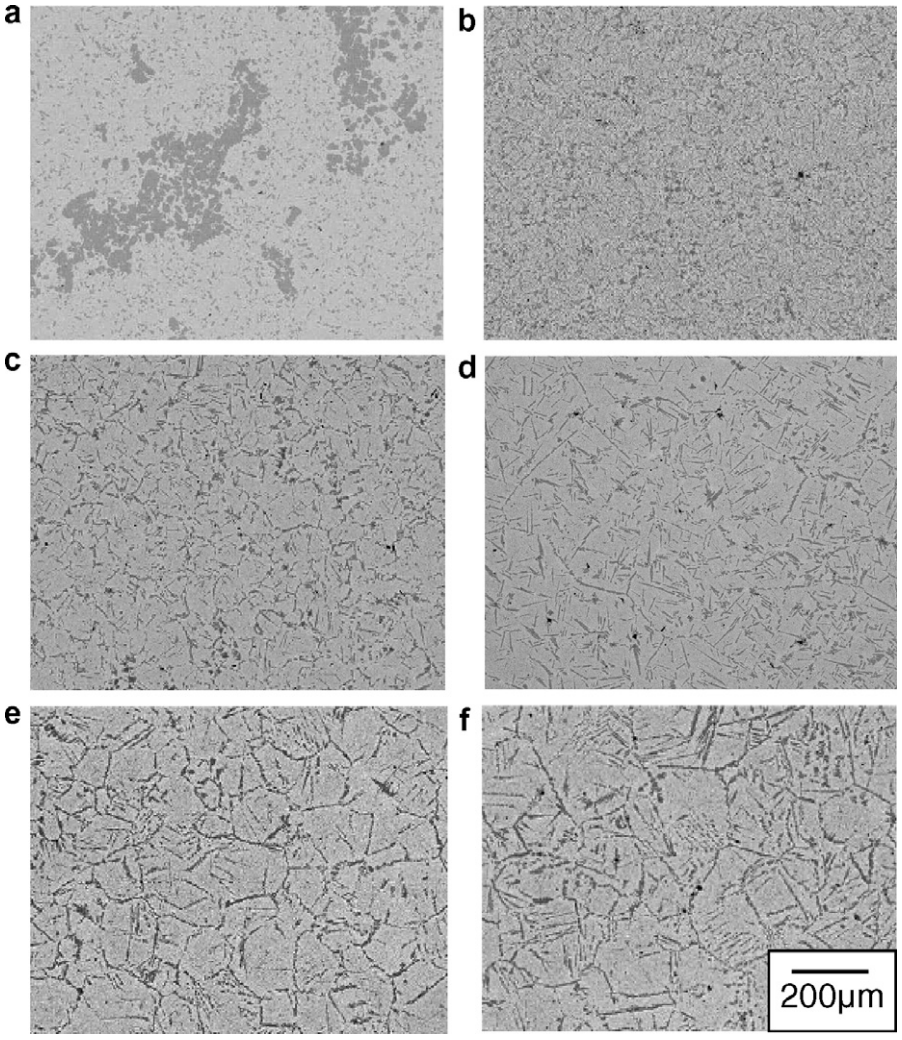

Fig. 6. Microstructures of the specimens sintered at (a) 1000 °C for 100 h, (b) 1300 °C for 30 h, (c) 1350 °C for 30 h, (d) 1400 °C for 10 h, (e) 1450 °C for 3 h, and (f) 1500 °C for 2 h.

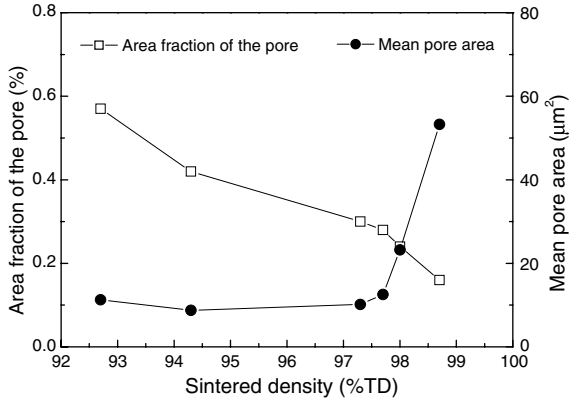

Fig. 7. Area fraction of the pore and the mean pore area with a sintered density.

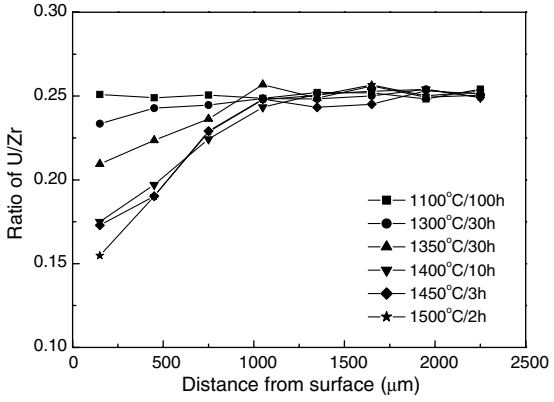

Fig. 8. Atomic ratio of U/Zr in the cross section of the sintered specimen.

this type in U–Pu–Zr alloys have been reported to be zirconium with impurities (O, N and C) in previous studies [6,7]. At a fast cooling rate of 10 °C/min, the massive Zr(O) grains, which were found at the slow cooling rate of 2 °C/min, were not observed, and the lath-type α-Zr precipitates were finely distributed throughout the matrix (Fig. 10(d)). These results indicate that a fast cooling from the sintering temperature could restrain the formation of the Zr(O) grains. A fast cooling rate also led to the increase

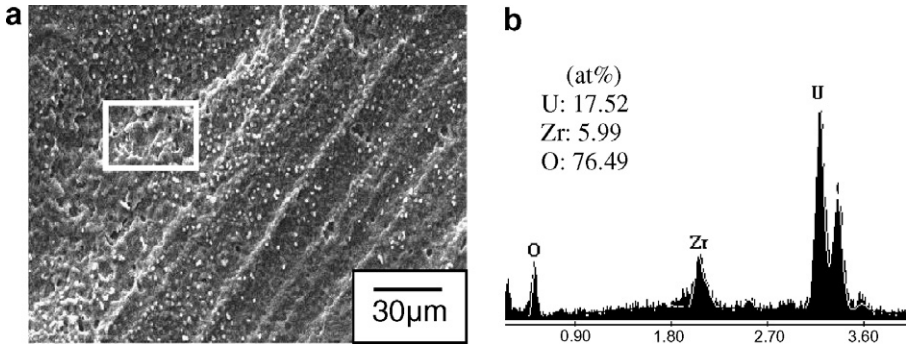

Fig. 9. SEM/EDS results of the deposits on the inner surface of the crucible after the sintering at 1500 °C for 2 h: (a) surface appearance and (b) spectrum of the marked area in (a).

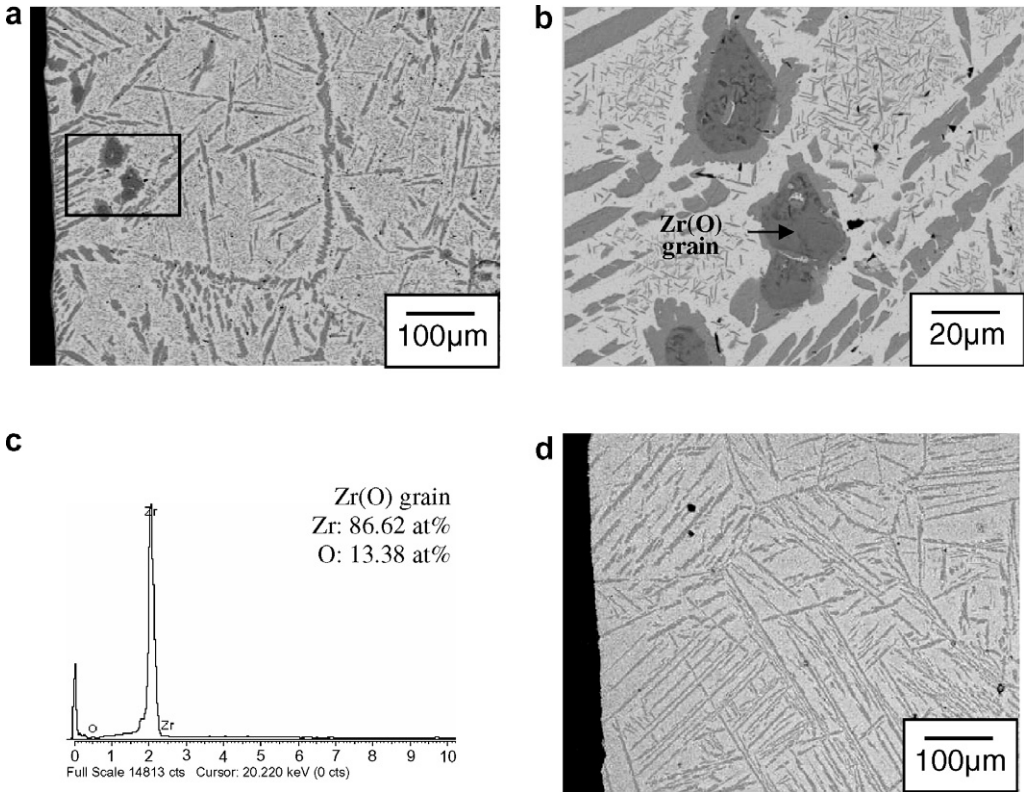

Fig. 10. Effect of the cooling rate from a sintering temperature of 1500 °C on the microstructure of the sintered specimen: (a) cooling rate of 2 °C/min, (b) Zr(O) grains at the periphery of the sintered specimen marked in (a), (c) spectrum from Zr(O) grain arrowed in (b), and (d) cooling rate of 10 °C/min.

in the hardness of the sintered specimen from 245 to 289 Hv.

4. Conclusions

U–80 at.%Zr powder compacts were sintered in a temperature range from 1100 to 1500 °C in a vacuum of 1×10^{-4} Pa. The sintered density depended more on the sintering temperature than on the sintering time. A sintering at 1100 °C left un-reacted zirconium particles in the sintered specimen. The specimens sintered at temperatures above 1300 °C consisted of the δ-UZr_2 matrix with acicular α-Zr precipitates. The pore coarsening accompanied the increase in the sintered density. Uranium depletion near the surface of the sintered specimen was observed due to a vaporization of the U–Zr powder compacts during a sintering. Massive Zr(O) grains, which was observed at the periphery of the sintered specimen with a slow cooling rate of 2 °C/min, were not detected when the cooling rate from the sintering temperature was increased to 10 °C/min.

Acknowledgements

This study was supported by Korea Science and Engineering Foundation (KOSEF) and Ministry of Science and Technology (MOST), Korean government, through its National Nuclear Technology Program.

References

[1] J.S. Kim, Y.S. Jeon, S.D. Park, B.C. Song, S.H. Han, J.G. Kim, Nucl. Eng. Tech. 38 (2006) 301.
[2] T.D. Massalski, J.L. Murrey, L.H. Bennett, H. Baker, Binary Alloy Phase Diagrams, American Society of Metals, Ohio, 1986, p. 2151.
[3] C.L. Yaws, Handbook of Vapor Pressure, Houston, Texas, 1994.
[4] W. Wang, D.R. Olander, J. Am. Ceram. Soc. 76 (1993) 1242.
[5] D.R. Olander, W. Wang, J. Nucl. Mater. 223 (1995) 28.
[6] Y.H. Sohn, M.A. Dayananda, G.L. Hofman, R.V. Strain, S.L. Hayes, J. Nucl. Mater. 279 (2000) 317.
[7] G.L. Hofman, R.G. Rahl, C.E. Lahm, D.L. Porter, Metall. Trans. A 21 (1990) 517.